Chemical Engineering Journal 110 (2005) 87–100

Chemical Engineering Journal

www.elsevier.com/locate/cej

A new approach to fluid separation modelling in the columns equipped with structured packings

A. Shilkin, E.Y. Kenig *

Department of Biochemical and Chemical Engineering, University of Dortmund, Emil-Figge-Str. 70, 44227 Dortmund, Germany

Received 13 December 2004; received in revised form 9 March 2005; accepted 11 March 2005

Abstract

An analogy between the flow patterns in real separation columns equipped with structured packing and film flow is used to develop a new modelling approach. The packing is represented as a bundle of channels with identical triangular cross section. The dimensions of the channels as well as their number are derived from the packing geometry. The channel inner surface is wetted by a liquid flowing downwards, whereas the rest of the volume is occupied by a countercurrent vapour flow. Both phases are assumed to be totally mixed at regular intervals, determined by the corrugation geometry of the packing. The mathematical model is based on a set of partial differential equations describing hydrodynamics and mass and heat transport phenomena. These equations are complemented by the conjugate boundary conditions at the phase interface. A numerical solution of the model yields velocity profiles as well as concentration and temperature fields throughout the column. The model is verified using experimental data for a binary distillation in a column equipped with Montz-Pak A3-500.

Keywords: Hydrodynamic analogy; Two-phase flow; Mass and heat transfer; Structured packing

1. Introduction

The general tendency of chemical engineering is to reach increased efficiency and capacity of separation units at possibly minimal cost. This has brought about a novel generation of column internals, providing enhanced mass transfer performance and relatively low pressure drop. Among these internals, corrugated packings of the regular type, also referred as *structured packings*, have gained a wide acceptance [1–4]. Over the years, serious efforts have been made regarding the choice of an appropriate packing material as well as the optimisation of the corrugated sheet geometry [4–6]. This can be achieved only if transport phenomena in the packings are properly understood, and, hence, the development of sound predictive models is required. The modelling accuracy strongly depends on the appropriate description of phase interactions. For the separation processes taking place in geometrically simple flows like films, jets, drops, etc., physical boundaries of the contacting phases can be spatially localised. In this case, the partial differential equations of convective mass and heat transfer offer the most rigorous way to describe the transport phenomena. However, even for the regular geometry provided by corrugated sheet structured packings, the exact localisation of the phase interface represents a difficult problem, due to intricate interphase interactions dictated by packing geometry and surface characteristics. Therefore, most often, the modelling of separation processes is accomplished with the traditional *stage concept* [7], either using the *equilibrium* or *rate-based stage* models.

2. Stage concept

2.1. Equilibrium stage model

The equilibrium stage model was largely used for the description of separation processes during the last century. Since 1893, after the first equilibrium stage model was put forward by Sorel [8], numerous publications have appeared in the literature, discussing different aspects of its further development and application [9]. Equilibrium stage model

* Corresponding author. Tel.: +49 231 755 2357; fax: +49 231 755 3035.
E-mail address: e.kenig@bci.uni-dortmund.de (E.Y. Kenig).

1385-8947/$ – see front matter © 2005 Elsevier B.V. All rights reserved.
doi:10.1016/j.cej.2005.03.018

Nomenclature

a_e	effective mass transfer area (m^2/m^3)
a_t	geometric area (m^2/m^3)
b	corrugation base on the plane normal to column axis (m)
b_{riv}	width of a rivulet (m)
b_0	corrugation base on the plane normal to channel direction (m)
B	widths of corrugated sheets in a packing segment (m)
$\boldsymbol{C}$	vector of concentrations ($kmol/m^3$)
C_E	correction factor for surface renewal
d_h	channel hydraulic diameter (m)
D	diffusion coefficient of a component (m^2/s)
$[D]$	square matrices of multicomponent diffusion coefficients (m^2/s)
D_{pac}	packing diameter (m)
F	rivulet flow rate in the x, y or z directions (m)
F-factor	$u_{Gs}\sqrt{\rho_G}$ ($Pa^{1/2}$)
g	acceleration of gravity (m/s^2)
h	corrugation height (m)
$(\Delta \boldsymbol{H})^T$	vector of heats of phase transition (J/kmol)
k	mass transfer coefficient (m/s)
ℓ	total channel length in a packing segment (m)
L	height of packing segment (m)
$[M]$	phase equilibrium matrix
n	number of corrugated sheets in a column cross section
P	pressure (Pa)
q	volumetric flow rate (m^3/s)
R_h	hydraulic radius of the triangular channel ($d_h/2$) (m)
Re	Reynolds number ($U_{Ge}s_0\rho/\mu$)
s	corrugation side on the plane normal to column axis (m)
s_0	corrugation side on the plane normal to channel direction (m)
Sc	Schmidt number ($\mu/\rho D$)
Sh	Sherwood number (kd_h/D)
S_e	wetted inner surface of channels (m^2)
S_t	total inner surface of channels (m^2)
t_e	exposure time (s)
T	temperature (K)
u	velocity vector (m/s)
u_{Gs}	superficial velocity of the gas phase (m/s)
U_{Ge}	effective velocity of the gas phase (m/s)
U_{Le}	effective velocity of the liquid phase (m/s)
w	total wetted area in a column cross section (m^2)
z	length of undisturbed laminar flow (m)

Greek symbols

α	gravity flow angle (°)
β	angle defined by Eq. (7) (°)
γ	crimp angle (°)
δ	liquid film thickness (m)
ϵ	angle defined by Eq. (8) (°)
θ	solid–liquid contact angle (°)
κ	thermal diffusivity (m^2/s)
λ	thermal conductivity (J/m s K)
μ	viscosity (Pa s)
ν	kinematic viscosity (m^2/s)
ρ	mass density (kg/m^3)
σ	surface tension (N/m)
ϕ	plane inclination angle (°)
φ	corrugations inclination angle (with respect to column axis) (°)
ψ	number of channels in a packing segment

Indices

G	gas phase
L	liquid phase

assumes that the streams leaving a stage are at thermodynamic equilibrium. This idealisation is usually far from real process conditions, and therefore, process equipment is designed using the "height equivalent to a theoretical plate" (HETP), a gross parameter including the influence of packing type, size and material.

The limitations of the equilibrium stage model have long been recognised. For a multicomponent mixture, the same HETP is assumed for all components, this value being constant through the packing height. The latter is in contradiction with the experimental evidence and may lead to a severe underdesign [7]. Moreover, this model is not able to consider the packing geometry characteristics, which play a key role in actual mass and heat transfer. Therefore, for kinetically controlled processes, it is very difficult to use the equilibrium stage model without significant loss of accuracy.

2.2. Rate-based stage model

The so-called rate-based stage model presents a different way to the modelling of separation processes, by directly considering actual mass and heat transfer rates [7,10]. A number of models fall into the general framework of the rate-based stage. In most cases the film [11] or penetration and surface renewal [12,13] models find application, whereas the necessary model parameters are estimated by means of correlations. In this respect, the film model appears advantageous due to numerous correlation data available in the literature (see, e.g. [14]).

According to the film model, all the resistance to mass transfer is concentrated in two thin films adjacent to the phase interface. The film thicknesses represent modelparameters

which can be estimated using the mass transfer correlations [7,15]. It is also postulated that the mass transfer occurs within these films solely by molecular diffusion and that outside the films, in the bulk fluid, the level of mixing is so high that all composition gradients disappear. Mass transfer occurs through the films in the direction normal to the phase interface, whereas both molecular diffusion and convection parallel to the interface are neglected. Contrary to the equilibrium stage model, thermodynamic equilibrium is assumed here only at the phase interface. The mass balances are established for each phase separately and related by means of component diffusion fluxes [7]. In the case of multicomponent separations, which are most commonly encountered in industrial practice, multicomponent diffusion in the film phases is described by the Maxwell–Stefan equations which can be derived on the basis of the kinetic gas theory [16–18].

Certainly, the accuracy of the film model depends heavily on the proper estimation of the film thicknesses. As mentioned above, they are calculated using the mass transfer correlations obtained either experimentally [14] or on the semi-theoretical basis [19–23]. In the next section, a closer look at several major approaches to estimation of internals-related parameters is given.

3. Estimation of internals-related parameters

The first comprehensive study on hydrodynamics and mass transfer performance of structured packings was carried out by Zogg [19] for Sulzer BX and Sulzer BY gauze packings. The purpose of his study was to correlate the specific geometric characteristics of the analysed packings with their mass transfer performance.

The model proposed in Ref. [19] is based on the observations of the gas flow phenomena in corrugated passages. The experiments were carried out in a plexiglas installation with transparent walls, reproducing two adjacent corrugated sheets of a structured packing. Based on observed flow patterns, the gas flow through corrugated passages is modelled by a hydrodynamically similar one, namely as a flow through a bundle of identical channels with the triangular cross section. Using this analogy, the average gas velocity in the channels and corresponding Reynolds number can be calculated.

The liquid motion over a packing surface is approximated by a flow of a planar laminar gravitational film (the so-called "gravity flow") over an inclined smooth surface. The gravity flow angle corresponds to a minimal angle with the column axis (see also Refs. [24,25]). To take into account disturbances caused by interactions between the liquid films flowing over adjusted corrugated sheets, the length of undisturbed laminar film is introduced as a correction factor for the calculation of the liquid mass transfer coefficient.

Later, a similar model for mass transfer in gauze packings was proposed by Bravo et al. [20] and further extended by Fair and Bravo [26] and Rocha et al. [27,28], to include the expected incomplete surface wetting for structured packings of the corrugated sheet type. The authors used earlier investigations of wetted-wall columns provided by Johnstone and Pigford [29] and considered the gas flow in structured packings as passing through a series of wetted-wall columns with the dimensions related to the actual angle and size of the corrugations (see Fig. 1). In compliance with this analogy, the gas mass transfer coefficient was determined by the known expression for wetted-wall columns [29]:

$$Sh_G = 0.0338(Re_G)^{0.8}(Sc_G)^{1/3} \quad (1)$$

In Eq. (1), the Reynolds number is determined based on the hydraulic diameter of the flow channel. For the liquid phase, the penetration theory [12] is applied, whereas the exposure time is taken equal to

$$t_e = \frac{s_0}{C_E U_{Le}} \quad (2)$$

corresponding to the time necessary for the liquid to pass over the corrugation side s_0 (see Fig. 1). The main differences as compared to the model proposed in Ref. [19] are another geometry of the channels (a combination of a diamond-shaped and a triangular channel), different treatment of the hydrodynamic picture and application of other correlations for mass transfer coefficients.

A further model for the liquid distribution, effective contact area and mass transfer performance of structured packings was proposed by Nawrocki et al. [21]. Liquid motion over packing surface is approximated by a flow of rivulets, i.e. narrow films, their width depending on packing surface tension and structure. The authors assumed that the rivulets split at each crossing of adjacent corrugated sheets into two parts, with the fraction P passing into the neighbouring channel and the fraction $(1 - P)$ remaining in the original channel (see Fig. 2). Furthermore, no mass transfer is supposed to occur between two sides of a corrugated sheet and no radial mixing at the crossings. When approaching the column wall, the liquid is partially reflected back into the packing and partially flows down the wall according to the factor P. After the flow distribution is established, the width of each rivulet is determined using the formula suggested by Shi and

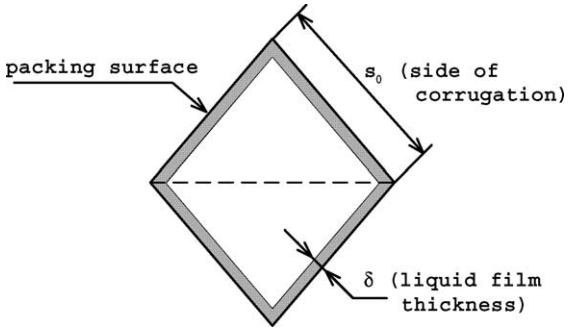

Fig. 1. Cross section of a flow channel (adapted from [27]).

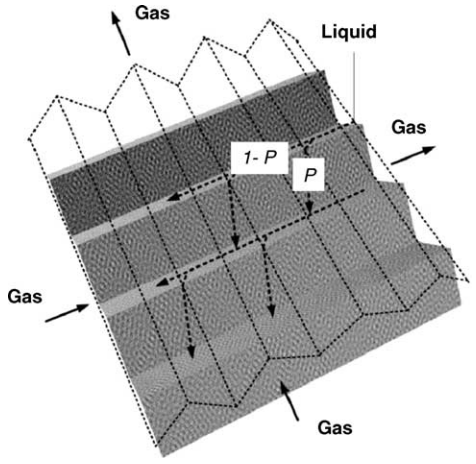

Fig. 2. Model of liquid distribution (adapted from [21]).

Mersmann [30]:

$$b_{\mathrm{riv}} = 3.49 F_{\mathrm{L}}^{0.4} \nu_{\mathrm{L}}^{0.2} \left(\frac{\rho_{\mathrm{L}}}{\sigma_{\mathrm{L}} g} \right)^{0.15} (1 - \cos\theta)^{-1} \quad (3)$$

whereas the effective wetted area of the structured packing is set equal to the total area of individual rivulets.

Following the common practice, Nawrocki et al. [21] adapted the Johnstone and Pigford [29] correlation for the calculation of the gas mass transfer coefficient, while for the liquid phase the penetration theory previously applied in Refs. [20,26] was utilised.

More recently, Olujić [31,32] reported an alternative model based on packing geometry for prediction of corrugated sheet structured packing separation performance. The model is grounded on a representation of a packing as a bundle of wetted wall channels with the characteristic triangular cross section, similar to the methods considered above. As in Refs. [26–28], liquid motion is approximated by the film flow over an inclined surface. Particular attention is given to several packing geometric characteristics, e.g. corrugation dimensions and inclination angle, which are explicitly taken into account in the model. A detailed comparison between the model, proposed in Refs. [26–28] and those reported in Refs. [31,32] was performed by Fair et al. [33]. The model suggested in Refs. [26–28] was judged as less amenable for further development since it is based on the fixed packing type and size specific parameters.

Another approach for predicting mass transfer performance of corrugated sheet structured packings was proposed by Aroonwilas and Tontiwachwuthikul [34]. Liquid motion through a packing is considered as a network of rivulets flowing over an inclined flat surface, merging and splitting at the crossing points between adjacent corrugated sheets. Furthermore, the flow from any given crossing point is assumed to be possible only in four directions (shown as q_1 to q_4 in Fig. 3) towards the crossing points at the lower level. The directions q_1 and q_2 correspond to the channel flow, whereas q_3 and q_4 to the gravity flow in the proportions dictated by the corrugated sheet perforation fraction. In the subsequent model development, the links between the possible flow directions and perforation properties are analysed more comprehensively [35].

After the flow rates of liquid rivulets from the crossing points have been determined with the above model, the width and average thickness of an individual rivulet can be estimated using the modified Shi and Mersmann approach [34] to enable calculations for varying inclination angle.

As usual, the authors resorted to the traditional technique for estimation of mass transfer characteristics, applying the penetration theory [12] and Eq. (1) suggested by Bravo et al. [20] for the liquid and gas phase mass transfer coefficients.

In such a way, all models discussed in this section are based on the rather simplified geometric consideration of the packing. They take into account only major geometric and surface characteristics which have a considerable impact on the process hydrodynamics. It is important that these models are simple enough to allow the application of continuum mechanics equations. However, the authors do not use this opportunity and resort to the traditional application of mass transfer coefficients in terms of the film model.

4. A closer look on the film model

Though widely used, the film theory reveals some problems, when applied to complex processes. A critical analysis shows, that the difficulties are mainly connected with the estimation of the film thickness. First, it is determined from the mass transfer correlations and therefore directly depends on the diffusion coefficients (cf. Eq. (1)). However, multicomponent mixtures are characterised by several diffusion coefficients related to different component binary pairs, and, therefore, the film thickness is different for each component. This leads to a formal contradiction, as, according to the film theory, the film thickness should be unique. Thus, in engineering practice this important model parameter has to be estimated as an average of component film thicknesses.

Another difficulty is related to convection, as, by definition, the films are stagnant and hence no mass transport

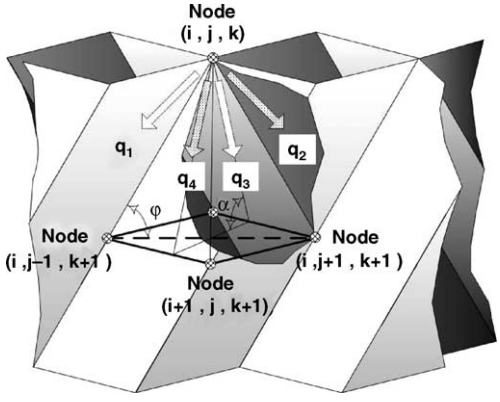

Fig. 3. Liquid distribution model (adapted from [34]).

mechanism, except for molecular diffusion in the direction normal to the interface, is possible [36]. Nevertheless, convection in films is directly accounted for in correlations. Moreover, in case of reactive systems, the film thickness should depend on the reaction rates, which cannot be considered in terms of this model.

The film theory, once developed for equimolar binary mass transfer in non-reactive systems [11], was free from contradictions. Nowadays, it is widely applied for much more complicated processes and therefore additional assumptions have to be made. These assumptions are in conflict with physical backgrounds and application of the model becomes problematic [36].

5. The idea of hydrodynamic analogy

The main reason for the application of simplified descriptions, as the film, penetration or surface renewal models is extremely complex hydrodynamics in the majority of industrial processes. When describing the hydrodynamics of such processes, it is hardly possible to localise the phase boundaries and specify the boundary conditions there. Therefore, the rigorous equations of continuum mechanics cannot be usually applied to the modelling of separation columns.

An opportunity to employ the rigorous equations of continuum mechanics even for the cases, in which real phase boundaries cannot be exactly localised, is associated with the idea of *hydrodynamic analogy* between complex and simpler flow phenomena. More precisely, some particular similarities are meant between complex flow patterns encountered in industrial separations and geometrically simple flows like films, jets, drops, etc. as well as their combinations [37]. Hydrodynamic analogies provide a means to process modelling, combining the rigour of exact continuum mechanics equations and rather simple geometric description.

An example of the hydrodynamic analogy is discussed in Ref. [37], where pertraction in falling liquid films is considered. This process represents a combination of extraction and re-extraction in a system comprising three liquid films flowing cocurrently, with the middle film being a liquid membrane [38,39]. The pertraction process is modelled basing on a simpler flow of parallel liquid films with constant thicknesses [40,41].

The hydrodynamic analogy idea has been also used for the modelling of zero-gravity distillation [42], where the real two-phase vapour–liquid mass transfer under countercurrent flow conditions is simulated by a film-flow approximation. To account for the change in the diffusion and hydrodynamic characteristics caused by the porous support used in this process, certain modifications of the governing equations are made. In all these examples, the simplified hydrodynamics allows the use of rigorous equations of continuum mechanics for the description of the separation units [36].

In the present paper, the hydrodynamic analogy idea is applied to rigorous modelling of distillation in columns equipped with structured packings. In the subsequent sections we discuss the modelling approach for the gas and liquid flows, mathematical description and the solution strategy.

6. Hydrodynamic analogy for structured packings

Generally, corrugated sheets structured packings are installed into a column as a bed of certain height and diameter. It is composed of a number of stacked elements (segments). The segments are perpendicular to each other to produce the mixing effects for both gas and liquid at each transition from one packing segment to another [23]. Each packing segment consists of a number of corrugated sheets manufactured from gauze, metal, ceramics or plastics and additionally mechanically or chemically treated to improve their wetting characteristics. A typical geometry of such corrugated sheets is sketched in Fig. 4.

The structured geometry of corrugated sheets results in a geometrically ordered fluid flow, which is different from the flow through random packings. The geometric characteristics of structured packings provide valuable information which helps to capture the gas and liquid flow patterns.

6.1. Gas flow

The corrugated sheets are installed counter course in such a way that they form channels crossing each other at a certain angle φ with column axis (see Fig. 4). Therefore, the packing segment can be visualised as a set of triangular flow channels, with identical cross sections and lengths dictated by the channel proximity to the column wall. Each channel is formed by the two wall sides s_0 and one open side b_0, which faces a neighbouring channel and is shared between the both channels [23].

Based on geometry and spatial arrangement of corrugated sheets and taking into account previous studies [19,21,27,31], we assume that the gas flow through a packing segment can be approximated by a flow through a bundle of channels with dimensions derived from the corrugation geometry (Fig. 4). For simplicity, we assume round channels, based on the widely used hydraulic diameter approximation. Furthermore,

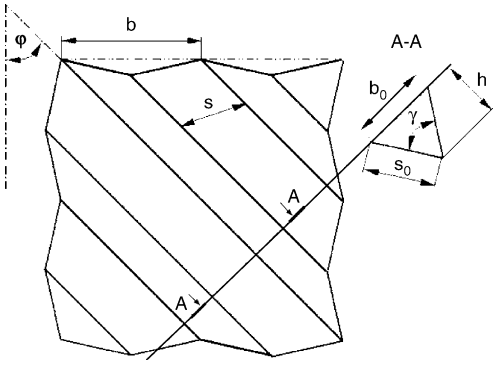

Fig. 4. Geometry of a corrugated sheet.

we consider the gas flow in the channels as laminar and fully developed, being ideally mixed at regular intervals [19,43]. The mixing points subdivide the laminar flow into fragments of a certain length. They are necessary to take into account the experimentally observed mixing of the gas flow due to an abrupt change in the gas flow direction towards the subsequent channel, either at the column wall or at a transition between the neighbouring packing segments. To be on line with experimental observations, we assume the length of the undisturbed laminar flow to be equal to an average channel length in a packing segment.

6.2. Liquid flow

The main purpose of corrugated sheet structured packings is to ensure continuous thin film flow [31]. In reality, the form of liquid flow over the packing surface is an intricate function of both liquid and surface properties as well as the packing geometry. A number of papers concerned with liquid flow over complex surfaces are available in the literature (see, e.g. Refs. [44–47]). Among others, a comprehensive experimental study of viscous film flow over various surfaces, similar to those encountered in industrial structured packings, was carried out by Zhao and Cerro [48] and Shetty and Cerro [49]. They discriminated between two types of structures to be associated to structured packings: macro-structure resulted from the corrugation geometry and micro-structure related to the packing material type and treatment. Further, they confirmed experimentally that liquid flow over structured packing surfaces can be approximated by a sequence of fully developed laminar viscous films flowing over flat surfaces with alternating inclinations.

According to experimental study of liquid flow over adjacent corrugated sheets under influence of gravity [50], liquids generally tend to move in form of laminar films at the minimal angle with the column axis, corresponding to the gravity flow angle α defined above.

Based on these considerations we assume that liquid motion over packing surface represents a laminar and fully developed film flow. This film wets the inner surface of the channels inclined in accordance with the gravity flow angle (see Fig. 5), whereas the rest of the volume is occupied by a countercurrent gas flow (see Section 6.1). We also assume, that for all channels, the film thickness is the same. This means that, at this stage, any radial maldistribution is neglected. Similar to the gas flow model, we apply the approximation of the periodic ideal mixing at regular intervals. However, the mixing in the liquid phase results from a different mechanism. Namely, since the gravity flow angle α does not coincide with the corrugation inclination angle φ, the liquid changes its flow direction abruptly when reaching a corrugation ridge. Thus, the length of the undisturbed laminar flow is assumed equal to the distance between the two neighbouring corrugation ridges [19]. The total inner surface of the channels represents a model parameter, which is calculated based on the packing wetted area.

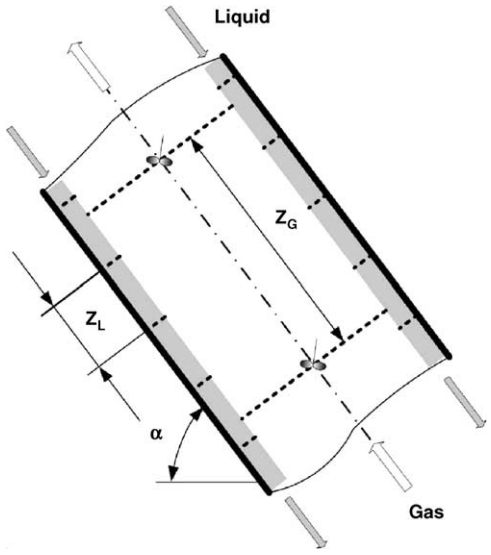

Fig. 5. Physical model for the flow structure (the mixing points are indicated by dash lines, z_L and z_G represent the lengths of undisturbed laminar liquid and gas flow, respectively).

7. Determination of the model parameters

According to the physical models for gas and liquid flows through corrugated sheet structured packing formulated in the previous section, laminar gas flow occurs through the bungle of inclined channels, whereas the liquid, in form of laminar films, wets their inner surface. The inner diameter of a channel is set equal to the hydraulic diameter of the corresponding triangular channel (see Fig. 4):

$$d_h = \frac{b_0 h}{s_0} \tag{4}$$

A schematic view of the flow in the channel is given in Fig. 6. The gravity flow angle α is calculated from the analysis of

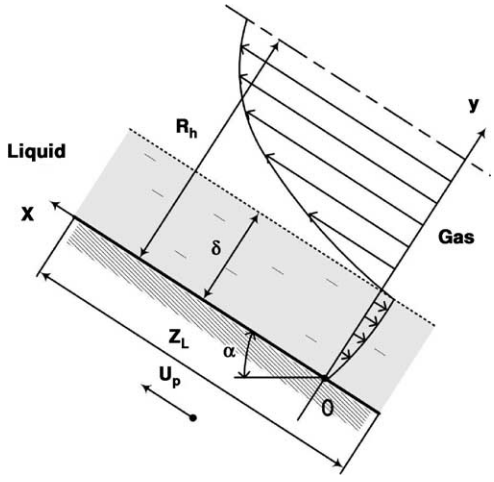

Fig. 6. Two-phase gas–liquid laminar countercurrent flow in a channel.

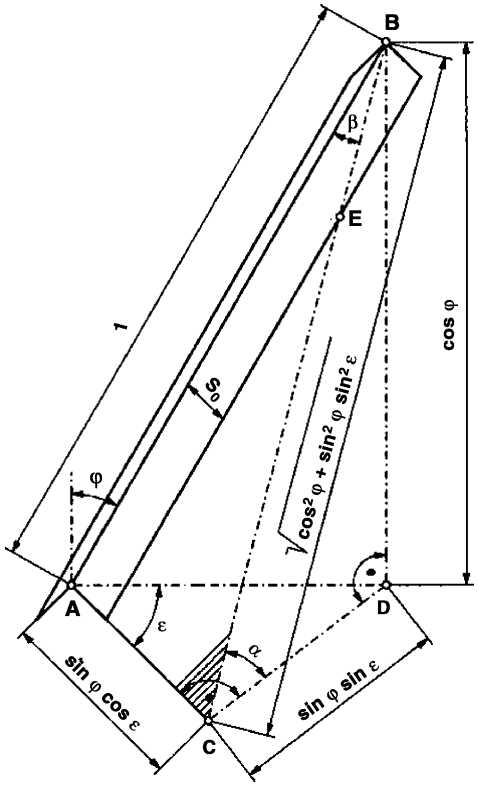

Fig. 7. To the calculation of the gravity angle (adapted from [19]).

a corrugated sheet single channel, with the length equal to unity (Fig. 7).

The segment BC represents an intersection of the plane BCD, normal to the base AC, and horizontal plane. Using the packing dimensions shown in Fig. 4, the following relation for the gravity angle can be derived [19]:

$$\alpha = \arctan\left(\frac{\cot\varphi}{\sin[\arctan(\cos\varphi\cot(\gamma/2))]}\right) \tag{5}$$

The length of undisturbed liquid laminar film flow corresponds to the interval BE and can be also derived from Fig. 7:

$$z_{\mathrm{L}} = \frac{b_0}{2\sin(\gamma/2)\sin\beta} \tag{6}$$

where

$$\beta = \arcsin(\sin\varphi\cos\epsilon) \tag{7}$$

$$\epsilon = \arctan(\cos\varphi\cot(\gamma/2)) \tag{8}$$

As mentioned above, the length of undisturbed laminar gas flow is equal to the average channel length in a packing segment. Total channel length of a corrugated sheet in the packing is related to its dimensions (see Fig. 8) by the following formula:

$$\ell_i = \frac{2B_iL}{b\cos\varphi} = \frac{2B_iL}{b_0}, \quad i = 1,\ldots,n \tag{9}$$

where n is an integer number representing the number of corrugated sheets in a column cross section (rounded off to the nearest smaller integer number):

$$n = \mathrm{int}\left(\frac{D_{\mathrm{pac}}}{h}\right) \tag{10}$$

The width of ith corrugated sheet B_i is calculated from the crimp height h and the packing diameter:

$$B_i = \sqrt{D_{\mathrm{pac}}^2 - (h(n-2(i-1)))^2}, \quad i = 1,\ldots,k \tag{11}$$

with

$$k = \tfrac{1}{2}n$$

due to symmetrical arrangement of the corrugated sheets. When n is an odd number, k is rounded off to the nearest bigger integer number and B_k represents the width of the central sheet.

It can be proven, that the number of channels built up by a single sheet is equal to

$$\psi_i = \frac{2B_i}{b} + \frac{2L\tan\varphi}{b} - 1 = \frac{2(B_i\cos\varphi + L\sin\varphi) - b_0}{b_0}, \quad i = 1,\ldots,n \tag{12}$$

The average channel length is defined as a ratio of the total channel length in a packing segment (see Fig. 8) and the number of the channels:

$$z_{\mathrm{G}} = \frac{\sum_{i=1}^{n}\ell_i}{\sum_{i=1}^{n}\psi_i} \tag{13}$$

For an even n, it follows from Eq. (13):

$$z_{\mathrm{G}} = \frac{2L\sum_{i=1}^{k}B_i}{2\cos\varphi\sum_{i=1}^{k}B_i + k(2L\sin\varphi - b_0)} \tag{14}$$

whereas for an odd n:

$$z_{\mathrm{G}} = \frac{2L\left(2\sum_{i=1}^{k-1}B_i + B_k\right)}{2\cos\varphi\left(2\sum_{i=1}^{k-1}B_i + B_k\right) + (2k-1)(2L\sin\varphi - b_0)} \tag{15}$$

The total inner surface of the channels comprising a packing segment is related to the packing geometric (installed) area

$$S_{\mathrm{t}} = a_{\mathrm{t}}\frac{\pi D_{\mathrm{pac}}^2}{4}L \tag{16}$$

whereas their wetted surface to the packing effective (wetted) mass transfer area

$$S_{\mathrm{e}} = a_{\mathrm{e}}\frac{\pi D_{\mathrm{pac}}^2}{4}L \tag{17}$$

8. Governing equations and solution strategy

8.1. Hydrodynamics

The hydrodynamic part of the problem is usually assumed independent of the heat and mass transfer part. Hence, is can be solved separately. The system of Navier–Stokes equations in the film flow approximation [51] (Fig. 6) can be presented as follows [36,40]:

$$\mu_p\left(\frac{\partial^2 u_p}{\partial y^2}\right) - \frac{\partial P_p}{\partial x} + g\rho_p \sin\alpha = 0,$$

$$\frac{\partial P_p}{\partial y} = 0, \quad p = \mathrm{L}, \mathrm{G} \tag{18}$$

From Eq. (18)

$$\frac{\partial P_\mathrm{L}}{\partial x} = \frac{\partial P_\mathrm{G}}{\partial x} = \text{constant} = \Delta P \tag{19}$$

The boundary conditions are [36,40]:

- on the wall

$$y = 0, \quad u_\mathrm{L} = 0 \tag{20}$$

- at the interface

$$y = \delta, \qquad u_\mathrm{L} = u_\mathrm{G}, \qquad \mu_\mathrm{L}\frac{\partial u_\mathrm{L}}{\partial y} = \mu_\mathrm{G}\frac{\partial u_\mathrm{G}}{\partial y} \tag{21}$$

- at the channel symmetry axis

$$y = R_\mathrm{h}, \quad \frac{\partial u_\mathrm{G}}{\partial y} = 0 \tag{22}$$

In addition to the boundary conditions, Eqs. (20)–(22), the mathematical description is supplemented by the flow conservation conditions:

$$q_\mathrm{L} = w_\mathrm{L}\int_0^\delta u_\mathrm{L}(y)\,\mathrm{d}y = \text{constant} \tag{23}$$

$$q_\mathrm{G} = w_\mathrm{G}\int_\delta^{R_\mathrm{h}} u_\mathrm{G}(y)\,\mathrm{d}y = \text{constant} \tag{24}$$

where

$$w_\mathrm{L} = S_\mathrm{e}\frac{\sin\alpha}{L} \tag{25}$$

and

$$w_\mathrm{G} = S_\mathrm{t}\frac{\sin\alpha}{L} \tag{26}$$

are the widths of the wetted and total area in a packing cross section, respectively.

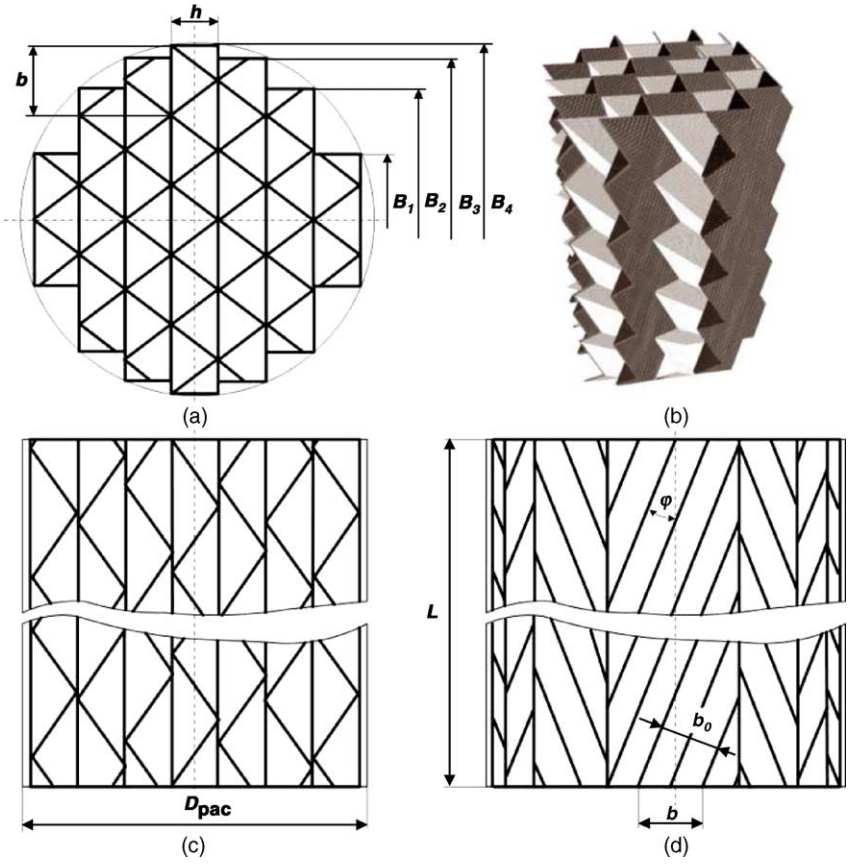

Fig. 8. Segment of a typical corrugated sheet structured packing ((a) top view, (b) isometric projection, (c) side view, (d) front view).

8.2. Solution of the hydrodynamic equations

The solution of Eq. (18) is a parabolic function:

$$u_p = A_p y^2 + B_p y + C_p, \quad p = \mathrm{L},\ \mathrm{G} \tag{27}$$

The coefficients A_p, B_p, C_p can be derived from the following relations resulted from the boundary and conservation conditions (Eqs. (20)–(24)):

$$A_\mathrm{L} = \frac{\Delta P + \rho_\mathrm{L} g \sin\alpha}{2\mu_\mathrm{L}} \tag{28a}$$

$$A_\mathrm{G} = \frac{\Delta P + \rho_\mathrm{G} g \sin\alpha}{2\mu_\mathrm{G}} \tag{28b}$$

$$B_\mathrm{G} = -2A_\mathrm{G} R_\mathrm{h} \tag{28c}$$

$$C_\mathrm{L} = 0 \tag{28d}$$

$$\mu_\mathrm{L}(2A_\mathrm{L}\delta + B_\mathrm{L}) = \mu_\mathrm{G}(2A_\mathrm{G}\delta + B_\mathrm{G}) \tag{28e}$$

$$A_\mathrm{L}\delta^2 + B_\mathrm{L}\delta = A_\mathrm{G}\delta^2 + B_\mathrm{G}\delta + C_\mathrm{G} \tag{28f}$$

$$q_\mathrm{L} = -w_\mathrm{L}\left(A_\mathrm{L}\frac{\delta^3}{3} + B_\mathrm{L}\frac{\delta^2}{2}\right) \tag{28g}$$

$$q_\mathrm{G} = w_\mathrm{G}\left(A_\mathrm{G}\frac{(R_h^3 - \delta^3)}{3} + B_\mathrm{G}\frac{(R_\mathrm{h}^2 - \delta^2)}{2} + C_\mathrm{G}(R_\mathrm{h} - \delta)\right) \tag{28h}$$

Combining Eqs. (28), the following expression for the determination of the liquid film thickness δ can be derived:

$$\frac{g w_\mathrm{G}\delta(R_\mathrm{h} - \delta)^2(\rho_\mathrm{L} - \rho_\mathrm{G})(3\mu_\mathrm{G}\delta + 4\mu_\mathrm{L}(R_\mathrm{h} - \delta))\sin\alpha}{6\mu_\mathrm{G}\mu_\mathrm{L}(3R_\mathrm{h} - \delta)} + \frac{q_\mathrm{L} w_\mathrm{G}(\delta - R_\mathrm{h})(3\mu_\mathrm{G}\delta(2R_\mathrm{h} - \delta) + 2\mu_\mathrm{L}(R_\mathrm{h} - \delta)^2)}{\mu_\mathrm{G} w_\mathrm{L}\delta^2(3R_\mathrm{h} - \delta)} - q_\mathrm{G} = 0 \tag{29}$$

Eq. (29) is solved numerically using Brent's method [52]. The values of the liquid film thickness δ obtained from Eq. (29) differ from those calculated from the well-known Nusselt approximation. This difference depends on the gas flow rate and may reach 10–25% for higher gas loads. Given the film thickness, solution of Eqs. (27) and (28) yields velocity profiles in both phases $u_p(y)$. These values are further used for the description of mass and heat transfer.

8.3. Simultaneous mass and heat transfer

To avoid difficulties connected with convergence and stability of calculations, the use of two different, oppositely directed reference frames in accordance with flow directions is advantageous [36]. Mass and heat transfer in each phase (Fig. 6) is described by the convective diffusion equations. Unlike the hydrodynamic part of the problem, the mass transfer part essentially depends on the number of components n and invokes the matrix equations when $n > 2$. To simplify the solution, we assume here that the channel curvature is negligible. Then the mass transfer equations are:

$$u_\mathrm{L}(y_1)\frac{\partial \boldsymbol{C}_\mathrm{L}}{\partial x_1} = [D_\mathrm{L}]\frac{\partial^2 \boldsymbol{C}_\mathrm{L}}{\partial y_1^2}, \qquad u_\mathrm{G}(y_2)\frac{\partial \boldsymbol{C}_\mathrm{G}}{\partial x_2} = [D_\mathrm{G}]\frac{\partial^2 \boldsymbol{C}_\mathrm{G}}{\partial y_2^2} \tag{30}$$

and the heat transfer equations are:

$$u_\mathrm{L}(y_1)\frac{\partial T_\mathrm{L}}{\partial x_1} = \kappa_\mathrm{L}\frac{\partial^2 T_\mathrm{L}}{\partial y_1^2}, \qquad u_\mathrm{G}(y_2)\frac{\partial T_\mathrm{G}}{\partial x_2} = \kappa_\mathrm{G}\frac{\partial^2 T_\mathrm{G}}{\partial y_2^2} \tag{31}$$

Boundary conditions are formulated as follows [36,40]:

- at the liquid entrance

$$x_1 = 0, \qquad \boldsymbol{C}_\mathrm{L} = \boldsymbol{C}_\mathrm{L}^0, \qquad T_\mathrm{L} = T_\mathrm{L}^0 \tag{32}$$

- at the gas entrance

$$x_2 = 0, \qquad \boldsymbol{C}_\mathrm{G} = \boldsymbol{C}_\mathrm{G}^0, \qquad T_\mathrm{G} = T_\mathrm{G}^0 \tag{33}$$

- at the wall (adiabatic and non-permeable)

$$y_1 = 0, \qquad \frac{\partial \boldsymbol{C}_\mathrm{L}}{\partial y_1} = 0, \qquad \frac{\partial T_\mathrm{L}}{\partial y_1} = 0 \tag{34}$$

- at the channel symmetry axis

$$y_2 = 0, \qquad \frac{\partial \boldsymbol{C}_\mathrm{G}}{\partial y_2} = 0, \qquad \frac{\partial T_\mathrm{G}}{\partial y_2} = 0 \tag{35}$$

- at the phase interface (thermodynamic equilibrium, mass and heat conservation conditions)

$$y_1 = \delta, \quad y_2 = R_\mathrm{h} - \delta; \qquad \boldsymbol{C}_\mathrm{G} = [M]\boldsymbol{C}_\mathrm{L}, \quad T_\mathrm{L} = T_\mathrm{G};$$
$$[D_\mathrm{L}]\frac{\partial \boldsymbol{C}_\mathrm{L}}{\partial y_1} = -[D_\mathrm{G}]\frac{\partial \boldsymbol{C}_\mathrm{G}}{\partial y_2};$$
$$\lambda_\mathrm{L}\frac{\partial T_\mathrm{L}}{\partial y_1} = -\lambda_\mathrm{G}\frac{\partial T_\mathrm{G}}{\partial y_2} + (\Delta \boldsymbol{H})^\mathrm{T}[D_\mathrm{L}]\frac{\partial \boldsymbol{C}_\mathrm{L}}{\partial y_1} \tag{36}$$

The periodic ideal mixing is incorporated into the boundary conditions in the following way: the total channel height is subdivided into equal fragments with the lengths z_L and z_G for the liquid and gas phase, respectively. At the entrance of each single interval of an undisturbed fluid flow, the temperature and concentration profiles are uniform with respect to the coordinates y_1 and y_2. This means that the concentrations and temperatures at the entrance into each subsequent interval are assigned constant values calculated as integral mean values of the concentration and temperature distribution at the exit of the preceding interval.

Solution of Eqs. (30)–(36) yields concentration and temperature fields in the liquid and gas phase that can be used for the determination of any arbitrary characteristics of the two-phase mass and heat transfer, e.g., component fluxes or average concentration and temperature profiles along the column [36].

8.4. Solution of mass and heat transfer equations

Eqs. (30)–(36) are solved numerically, using the solution method similar to that suggested in Refs. [36,53]. The initial system of equations is reduced to an uncoupled (scalar-type) form and discretised by an implicit finite difference scheme. The resulting system is solved by the Thomas algorithm [54] with the use of the matrix-form coupled boundary conditions at the phase interface, Eq. (36).

This solution method is advantageous because of its simple implementation and stable performance. Contrary to the commonly used variations of the Newton's method, the Thomas algorithm allows a consecutive solution and – what is most important – does not depend on the choice of starting values.

9. Model verification

9.1. Experimental data

The proposed modelling approach has been verified using the total reflux distillation data for the binary mixture chlorobenzene/ethylbenzene (CB/EB) obtained at the University of Dortmund [55]. The experiments were carried out in a column of 100 mm inner diameter, equipped with structured packing Montz-Pak A3-500. The geometric characteristics of this packing are given in Table 1. The packing was installed in 1 m high beds, with the total height of 3 m. The experiments were accomplished for operating conditions changing in a wide range in order to reveal the area of model application regarding the assumptions made.

For each packing section of 1 m height, the samples were taken at three locations: 0.1, 0.5 and 0.9 m. Moreover, probes were taken above and below the packing sections as well as from the reflux and bottom streams. All samples were analysed off-line with a gas chromatograph. Absolute pressure at the top of the column was measured by pressure transducers. The distillate flow rate was determined by coriolis-mass-flow-meter, whereas the bottom flow rate was measured by a graduated glass using a stop watch.

9.2. Model implementation

The model described in Section 8 and the solution algorithms have been implemented in FORTRAN. The routines are arranged in two modules covering hydrodynamic and simultaneous mass and heat transfer calculations. The necessary physical data are calculated using Aspen Properties® data base [56]. To access the properties data base, the written routines are compiled and linked into a shared library via Aspen simulation engine. This allows automatic loading and execution of the FORTRAN files directly from Aspen Plus® interface during simulation runs. The FORTRAN code has been developed in a general way to allow any arbitrary modification of the component list (including the number of components) as well as the physical property calculation methods from Aspen Plus® without recompilation of the FORTRAN code. Complementary to our own model, the built-in FLASH2 model [56] is used for the modelling of the column reboiler.

Table 1
Geometric characteristics of Montz-Pak A3-500

a_t (m^2/m^3)	500
ϵ (–)	0.95
h (m)	0.006
b_0 (m)	0.009
s_0 (m)	0.0075
L (m)	0.183
γ (°)	74
φ (°)	30

Table 2
Model parameters

d_h (m)	0.0045
α (°)	66.5
z_L (m)	0.0228
z_G (m)	0.0965
S_t (m^2)	0.718
S_e (m^2)	0.718

9.3. Simulations

In the simulations, the average concentration and temperature profiles were obtained based on the calculated local concentration and temperature fields. The measured concentration, temperatures and flow rates at the condenser outlet were used as input parameters. Our purpose was to reproduce the measured concentration profiles along the column. The packing specific model parameters calculated with the use of Eqs. (4)–(16) are summarised in Table 2. Since the gauze packings generally exhibit a very good wetting performance, the packing surface was assumed to be fully wetted.

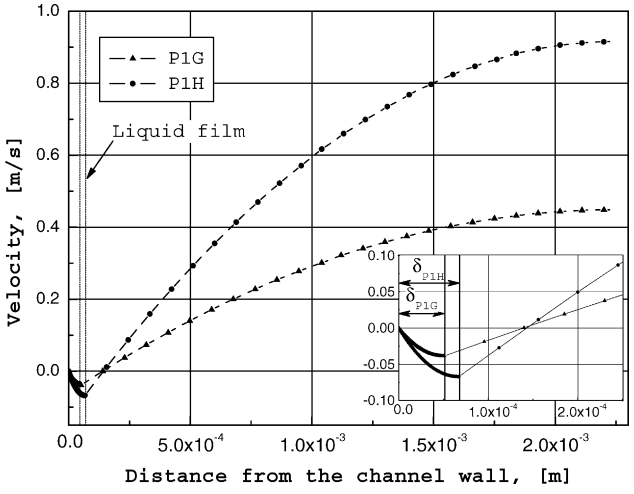

Fig. 9. Calculated velocity profiles for two different operating conditions (P1G: $q_L = 0.0277\,m^3/h$, $T_L^0 = 384.15\,K$, $x_0(CB) = 0.8944$; P1H: $q_L = 0.0575\,m^3/h$, $T_L^0 = 393.15\,K$, $x_0(CB) = 0.8220$).

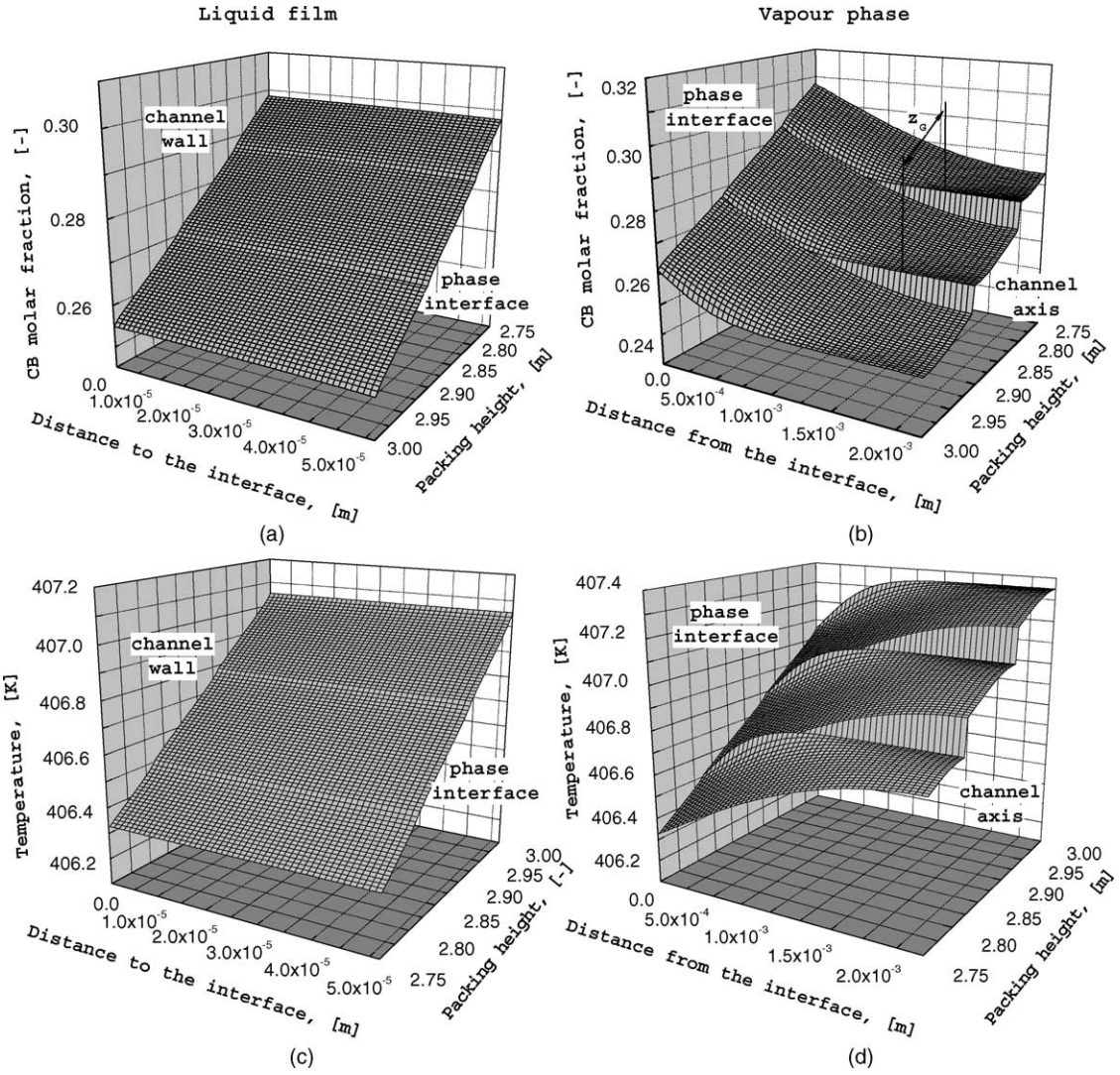

Fig. 10. Calculated concentrations of chlorobenzene (a,b) and mixture temperature (c,d) for the lower 0.25 m part of the column ($q_L = 0.0277\ m^3/h$, $x_0(CB) = 0.8944$, total packing height = 3 m).

Fig. 9 shows the velocity profiles resulted from the solution of the hydrodynamic equations (see Section 8.1) for two different experiments. In these experiments, the flow rates are such that the interfacial shear stresses take relatively small values resulting in the observed semi-parabolic velocity profiles for both phases. A strong influence of the liquid flow on the vapour flow can be observed, namely, there are negative velocities indicating the reverse vapour flow, clearly seen in the enlarged fragment in Fig. 9. Increasing the vapour flow rate results in a rapid grow of the liquid film thickness δ, since the vapour slows down the flowing liquid and, hence, makes it thicker.

Fig. 10 demonstrates the chlorobenzene concentration and temperature fields in the neighbouring liquid and vapour phases for the lower part of the column. To render the trends presented here clearly to the reader, the packing height axes for concentration ((a) and (b)) and temperature ((c) and (d)) fields are orientated oppositely. The concentration gradients in the vapour phase are significantly higher and concentration profiles steeper than in the liquid phase. Obviously, the influence of the regular mixing manifested in form of the stepwise changes in the concentration and temperature is much more pronounced in the vapour phase (see (b) and (d)). It should be pointed out that the same trends observed in the liquid phase are caused by the mixing in the vapour phase. Influence of ideal mixing on the concentration field in the liquid phase cannot be noticed at given conditions. This can be explained by the prevailing resistance to the mass transfer in the vapour phase which is typical for distillation.

9.4. Comparison with experimental data

In Fig. 11, the calculated concentration profiles for chlorobenzene are compared with measured data. Simulations are carried out for two different operating pressures, when *F*-factor calculated under the packing ranges from

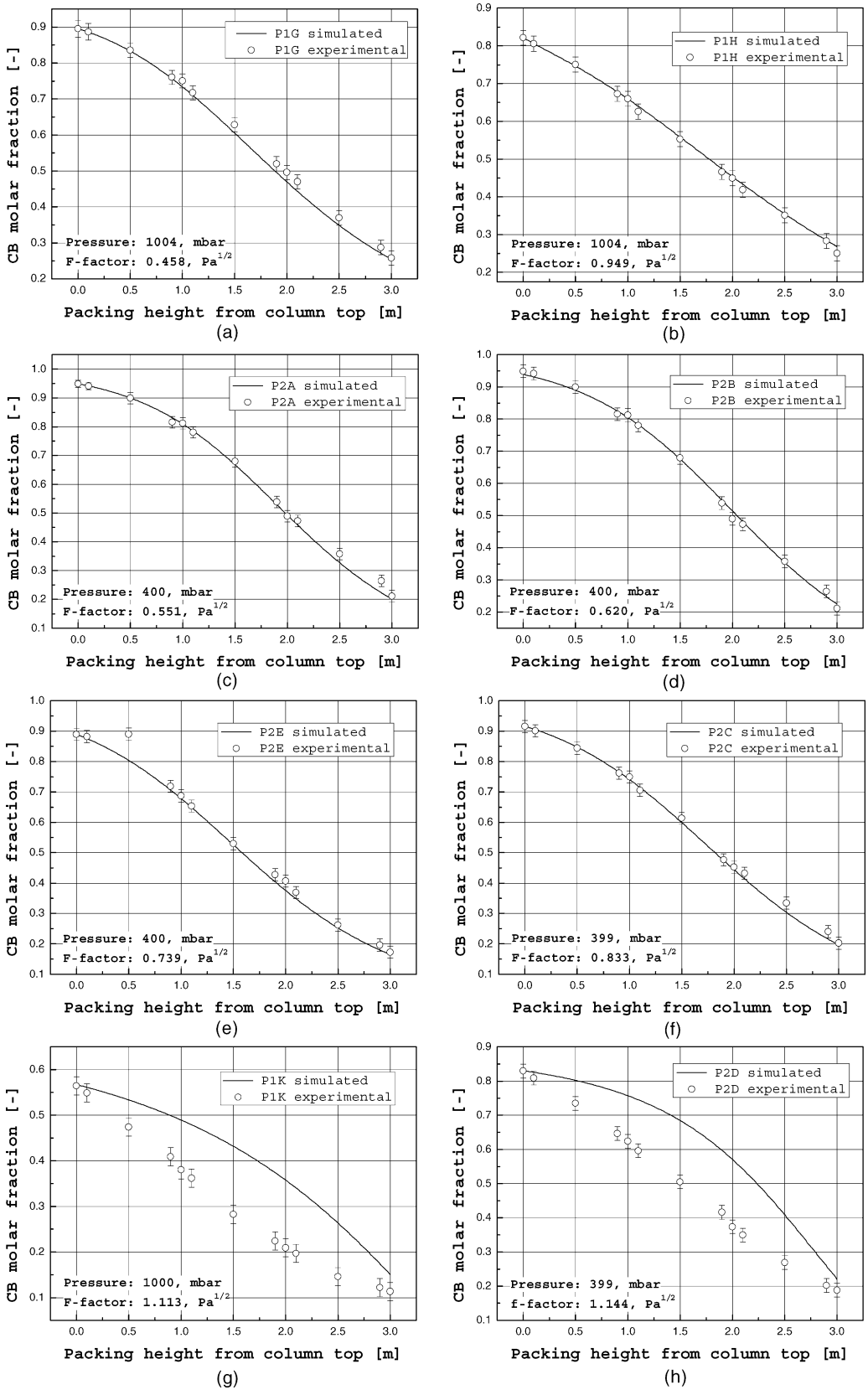

Fig. 11. Comparison of calculated and experimentally obtained chlorobenzene (CB) concentration profiles.

0.458 to 1.144 $Pa^{1/2}$. Under the total reflux conditions, an increase in the gas flow rate implies a corresponding increase in the liquid load. For the given operating conditions, the values of liquid phase Reynolds numbers varied through a small range up to 30, which corresponds to viscous laminar flow with constant film thickness.

Based on the comparison shown in Fig. 11, some conclusions regarding the range of application of the proposed model can be drawn. Fig. 11 demonstrates a very good agreement between the predicted and measured data in the range of *F*-factor up to approximately 1.0, whereas for higher values, the discrepancy between the calculated and measured concentrations becomes considerable (see Fig. 11g–h). Further simulation studies showed that this discrepancy increases with increased *F*-factor, even at constant values of the liquid load. The latter suggests that at the values of *F*-factor starting from 1.0, the gas flow in channels attains a behaviour strongly deviating from the laminar flow assumed in the model. It can be concluded that even under assumption of regular total mixing of the vapour phase, the model fails to predict the mass transfer performance at the transitional flow regime. From Fig. 10b it is evident that the vapour phase experiences a very intensive mixing and this effect cannot be fully mirrored by considering the total mixing at channel transitions.

10. Conclusions

A new approach to rigorous modelling of separation processes has been applied to modelling of columns equipped with corrugated sheet structured packings. This approach is based on the hydrodynamic analogy between real complex hydrodynamics dominating most industrial separations and geometrically simpler flow patterns.

The physical model gives a simplified geometric representation of the packing. It consists of a bundle of channels with identical triangular cross section. The inner surface of these channels is wetted by a liquid flowing downwards, whereas the rest of the volume is occupied by a countercurrent vapour flow. Both flows are presumed to be laminar and fully developed within intervals of a certain length, being totally mixed between them. The interval lengths for each phase represent the packing specific model parameters and are derived from the packing geometry. This simplified hydrodynamic picture allows an exact localisation of the phase boundaries, which permits a direct application of continuum mechanics equations.

The hydrodynamic part of the problem is assumed to be independent of the mass and heat transfer and solved separately. It comprises the Navier–Stokes equations in the film-flow approximation for both phases supplemented by the conjugate boundary conditions at the phase interface. Solution of the equations system yields velocity profiles and the liquid film thickness.

Mass and heat transfer phenomena are described by the partial differential equations of convective diffusion and heat conduction. Similar to the hydrodynamic problem, these equations are applied to both phases and coupled by the boundary conditions at the phase interface. The solution gives local concentration and temperature fields, which are used for calculation of the concentration and temperature profiles along the column.

The proposed model has been verified using the total reflux distillation data for binary mixture chlorobenzene/ethylbenzene in the column, equipped with the Montz-Pak A3-500 structured packing. The comparison of the calculated and measured concentrations shows a very good agreement for values of *F*-factor corresponding to laminar flow regime, what is in accordance with the assumptions of the model. Next objective is to extend the approach to transitional and turbulent flow regimes for the vapour phase. The model will be tested for different packings and multicomponent systems at relevant operating conditions.

Acknowledgement

The support of Stiftung Stipendien-Fonds des Verbandes der Chemischen Industrie e.V. is greatly acknowledged.

References

[1] A. Sperandio, M. Richard, M. Huber, Eine Neue Packung fur die Vakuumrektifikation, Chem.-Ing.-Tech. 3 (1965) 322–328.
[2] M. Sakata, Tests of 1000, 250 and 70 mm diameter columns with Koch Sulzer packing, Technical Report No. 22, Fractionation Research, Inc., February 15, 1972.
[3] L. Spiegel, W. Meier, Distillation column with structured packings in the next decade, Trans. IChemE 81 (2003) 39–47.
[4] G.K. Chen, L. Kitterman, J.H. Shieh, Develoment of a new generation of high efficiency packing for mass transfer operations, Chem. Eng. Prog. 79 (1982) 48.
[5] K. McNulty, C.L. Hsieh, Hydraulic performance and efficiency of Koch Flexipac structured packing, in: Proceedings of the AIChE National Meeting, November, 1982.
[6] Ž. Olujić, H. Jansen, B. Kaibel, T. Rietfort, E. Zich, Stretching the capacity of structured packings, Ind. Eng. Chem. Res. 40 (2001) 6172–6180.
[7] R. Taylor, R. Krishna, Multicomponent Mass Transfer, Wiley, 1993.
[8] E. Sorel, La Rectification de L'alcool, Gauthiers - Villais et fils, 1893.
[9] E.J. Henley, J.D. Seader, Equilibrium Stage Separation Operations in Chemical Engineering, Wiley, New York, 1981.
[10] J.D. Seader, The rate-based approach for modelling staged separations, Chem. Eng. Prog. 85 (1989) 41–49.
[11] W.K. Lewis, W.G. Whitman, Principles of gas absorption, Ind. Eng. Chem. 16 (1924) 1215–1220.
[12] R. Higbie, The rate of absorption of a pure gas into a still liquid during shot periods of exposure, Trans. Am. Inst. Chem. Eng. 31 (1935) 365–383.
[13] P.V. Danckwerts, Significance of liquid-film coefficients in gas absorption, Ind. Eng. Chem. 43 (1951) 1460–1467.
[14] R. Billet, M. Schultes, Prediction of mass transfer columns with dumped and arranged packings: updated summary of the calculation method of Billet and Schultes, Trans. IChemE 77 (1999) 498–504.

[15] T.K. Sherwood, R.L. Pigford, C.R. Wilke, Mass Transfer, McGraw-Hill, New York, 1975.
[16] J.O. Hirschfelder, C.F. Curtiss, R.B. Bird, Molecular Theory of Gases and Liquids, Wiley, New York, 1964.
[17] H.L. Toor, Solution of the linearized equations of multicomponent mass transfer. II. Matrix methods, AIChE J. 10 (1964) 460–465.
[18] W.E. Stewart, R. Prober, Matrix calculation of multicomponent mass transfer in isothermal systems, Ind. Eng. Chem. Fund. 3 (1964) 224–235.
[19] M. Zogg, Stromungs- und Stoffaustauschuntersuchungen an der Sulzer-Gewebepackung. Ph.D. thesis, Technische Hochschule Zurich, 1972.
[20] J.L. Bravo, J.A. Rocha, J.R. Fair, Mass transfer in gauze packing, Hydrocarb. Process. (1985) 91–95.
[21] P.A. Nawrocki, Z.P. Xu, K.T. Chuang, Mass transfer in structured packing, Can. J. Chem. Eng. 69 (1991) 1336–1343.
[22] E. Brunazzi, A. Paglianti, Liquid-film mass transfer coefficient in a column equipped with structured packing, Ind. Eng. Chem. Res. 36 (1997) 3792–3799.
[23] Ž. Olujić, A.B. Kamerbeek, J. Graauw, A corrugation geometry based model for efficiency of structured distillation packing, Chem. Eng. Process. 38 (1999) 683–695.
[24] M. Zogg, Modifizierte Stoffubergangskoeffizienten fur Bilanzmäβige Stoffiibergangsberechnungen an laminaren Rieselfilmen, Chem. -Ing. -Tech. 44 (1972) 930–936.
[25] M. Zogg, Stoffaustausch in der Sulzer-Gewebepackung, Chem.-Ing.-Tech. 45 (1973) 67–74.
[26] J.R. Fair, J.L. Bravo, Distillation columns containing structured packings, Chem. Eng. Prog. (1990) 19–29.
[27] J.A. Rocha, J.L. Bravo, J.R. Fair, Distillation columns containing structured packings: a comprehensive model for their performance. 1. Hydraulic models, Ind. Eng. Chem. Res. 32 (1993) 641–651.
[28] J.A. Rocha, J.L. Bravo, J.R. Fair, Distillation columns containing structured packings: a comprehensive model for their performance. 2. Mass-transfer model, Ind. Eng. Chem. Res. 35 (1996) 1660–1667.
[29] H.F. Johnstone, R.L. Pigford, Distillation in a wetted-wall column, Trans. Am. Inst. Chem. Eng. 38 (1942) 25–50.
[30] M.G. Shi, A. Mersmann, Effective interfacial area in packed columns, German Chem. Eng. 8 (1985) 87–96.
[31] Ž. Olujić, Development of a complete simulation model for predicting the hydraulic and separation performance of distillation columns equipped with structured packings, Chem. Biochem. Eng. Quart. 11 (1) (1997) 31–46.
[32] Ž. Olujić, Effect of column diameter on pressure drop of a corrugated sheet structured packing, Chem. Eng. Res. Des. 77 (6) (1999) 505–510.
[33] J.R. Fair, A.F. Seibert, M. Behrens, P.P. Saraber, Ž. Olujić, Structured packing performances – experimental evaluation of two predictive models, Ind. Eng. Chem. Res. 39 (2000) 1788–1796.
[34] A. Aroonwilas, P. Tontiwachwuthikul, Mechanistic model for prediction of structured packing mass transfer performance in CO_2 absorption with chemical reaction, Chem. Eng. Sci. 55 (2000) 3651–3663.
[35] A. Aroonwilas, A. Chama, P. Tontiwachwuthikul, A. Veawab, Mathematical modelling of mass-transfer and hydrodynamics in CO_2 absorbers packed with structured packings, Chem. Eng. Sci. 58 (2003) 4037–4053.
[36] E. Kenig, Modeling of Multicomponent Mass Transfer in Separation of Fluid Mixtures, VDI-Verlag, Diisseldorf, 2000.
[37] E.Y. Kenig, Multicomponent multiphase film-like systems: a modeling approach, Comput. Chem. Eng. 21 (1997) S355–S360.
[38] L. Boyadzhiev, Liquid pertraction or liquid membranes - state of the art, Sep. Sci. Technol. 25 (1990) 187–205.
[39] Z. Lazarova, L. Boyadzhiev, Liquid film pertraction – a liquid membrane preconcentration technique, Talanta 39 (1992) 931–935.
[40] L.P. Kholpanov, K.V. Avetisyan, V.A. Malysov, Fluid mechanics and mass transfer during three-phase membrane extraction, Theor. Found. Chem. Eng. 22 (1988) 299–305.
[41] E.Y. Kenig, L.P. Kholpanov, V.A. Malyusov, Calculation of three-phase liquid extraction parameters in multicomponent mixtures, Proc. Acad. Sci. USSR, Chem. Technol. Section 313 (1990) 83–86.
[42] J. Tschernjaew, E.Y. Kenig, A. Górak, Mikrodestillation von Mehrkomponentensystemen, Chem.-Ing.-Tech. 68 (1996) 272–276.
[43] G.F. Versteeg, J.B.M. Visser, L.L. Van Dierendonck, J.A.M. Kuipers, Absorption accompanied with chemical reaction in trickle-bed reactors, Chem. Eng. Sci. 52 (1997) 4057–4067.
[44] G.D. Fulford, The flow of liquids in thin films, Adv. Chem. Eng. 5 (1964) 151–236.
[45] C.Y. Wang, Liquid film flowing slowly down a wavy incline, AIChE J. 27 (1981) 207–212.
[46] C. Pozrikidis, The flow of a liquid film along a periodic wall, J. Fluid Mech. 188 (1988) 275–300.
[47] Yu.Ya. Trifonov, Viscous liquid film flows over a periodic surface, Int. J. Multiphase Flow 29 (1999) 1139–1161.
[48] L. Zhao, R.L. Cerro, Experimental characterization of viscous film flows over complex surfaces, Int. J. Multiphase Flow 18 (1992) 495–516.
[49] S. Shetty, R.L. Cerro, Flow of a thin film over a periodic surface, Int. J. Multiphase Flow 19 (1993) 1013–1027.
[50] F. Stoter, Modeling of maldistribution in structured packings: from detail to column design, Ph.D. Thesis, Delft University of Technology, 1993.
[51] G. Levich, Physicochemical Hydrodynamics, Prentice-Hall, Englewood Cliffs, NJ, 1962.
[52] R.P. Brent, An algorithm with guaranteed convergence for finding a zero of a function, Comput. J. 14 (1971) 422–425.
[53] L.P. Kholpanov, E.Y. Kenig, V.A. Malyusov, Calculation of combined heat and mass transfer in countercurrent gas–liquid film flow, J. Eng. Phys. 51 (1986) 768–773.
[54] S.V. Patankar, Numerical Heat Transfer and Fluid Flow, Hemisphere Publ. Corp./McGraw-Hill, New York, 1980.
[55] S. Pelkonen, Multicomponent mass transfer in packed distillation columns, Ph.D. Thesis, University of Dortmund, 1997.
[56] User Models, Version 11.1, Aspen Technology, Inc., August 2001.